Journal of Statistical Physics, Vol. 17, No. 3, 1977

Structure of a Liquid–Vapor Interface

M. H. Kalos,[1] J. K. Percus,[1,2] and M. Rao[1,3,4]

Received December 30, 1976; revised February 24, 1977

The structure of the interface of an argonlike fluid in equilibrium with its own vapor at low temperature is studied using molecular dynamics. The longitudinal pair correlations in the interface are found to be consistent with a simply defined ensemble of local thermodynamic states. However, the transverse correlations exhibit very long-range behavior not predicted by straightforward local thermodynamics. These results strongly suggest that the interface is made up of an ensemble of configurations in each of which the transition from liquid to vapor is locally sharp, but that the transition surface fluctuates strongly in space and time.

KEY WORDS: Liquid–vapor interface; liquid argon; capillary waves.

1. INTRODUCTION

Since the inception of statistical mechanics the structure of the transition zone between liquid and vapor in equilibrium has been of great theoretical interest.[5] From a thermodynamic viewpoint, surface-associated quantities such as surface tension fit without difficulty into a framework encompassing the variation of both bulk and surface parameters (see, e.g., Ref. 2). But the jump from a microscopic description of structure in bulk fluid to that in the interface region has long eluded reliable analysis. This is largely because the experimental information so necessary to direct theoretical efforts remains very meager. There are relatively few equivalent particles entering into any given aspect of the interface, and their contributions to physical measurements are masked by the background from bulk particles.

Supported in part by ERDA, Contract No. EY-76-C-02-3077, and by NSF, Grant DMR-72-03029, through Materials Science Center, Cornell University.

[1] Courant Institute of Mathematical Sciences, New York University, New York, New York.

[2] Department of Physics, New York University, New York, New York.

[3] Laboratory of Atomic and Solid State Physics, Cornell University, Ithaca, New York.

[4] Present address: Chemistry Department, Columbia University, New York, New York.

[5] The classical theoretical density profile dates back to van der Waals.[1]

The advent of modern digital computers has changed this situation. Now it is possible to perform a numerical simulation of an equilibrium system with a large proportion of interface particles,[3] and sufficiently many to ensure good statistics not only for density computation, but even for joint distributions of particle pairs. With this information, one can begin to evaluate various theoretical approximations and suggestive concepts, and, more importantly, provide a suitable qualitative framework for the microscopic phenomenology of two-phase fluid interfaces.

In this paper, we will study an argonlike fluid at low temperature. It is now fairly well established[4,5] that for a planar two-phase interface, the density profile $\rho(z)$ is a smooth, monotone function approaching the corresponding liquid or vapor density in the one-phase regions (see Fig. 1 for a profile from data of this paper). The common ingredient of theoretical derivations of $\rho(z)$ has always been some Ansatz for relating the pair distribution function $\rho^{(2)}(\mathbf{r}_1, \mathbf{r}_2)$ to $\rho(z)$ and a suitable bulk pair distribution. In the present analysis, we first investigate the longitudinal pair correlations and show that they are consistent with a simply defined ensemble of local thermodynamic states. Self-consistent use of this idea, however, produces a density profile substantially steeper than the numerically observed $\rho(z)$.

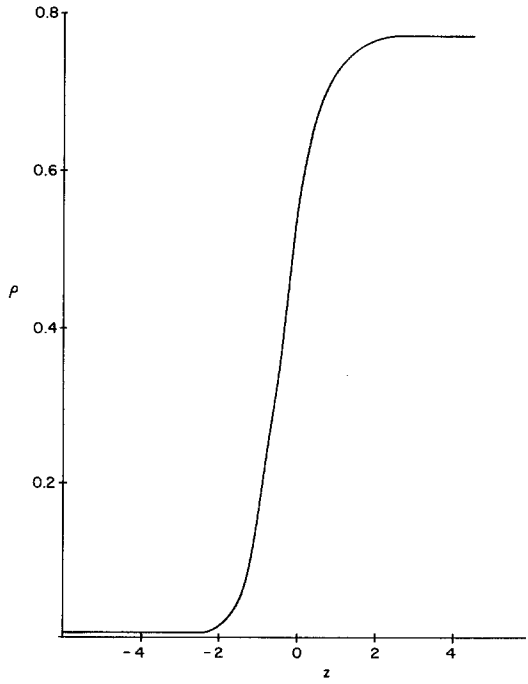

Fig. 1. Density profile for model argon at 84°K (units as in text).

We next proceed to transverse correlations, via a transverse Fourier transform, and find that they exhibit very long-range behavior not predicted by naive local thermodynamics. This behavior is shown to be a quite general consequence of the existence of a self-supported phase transition region, and is placed dynamically in the context of ensembles of wavelike gas–liquid interfaces. The observed broadening of the density profile has a similar origin. To exhibit the genesis of the transverse correlations, an intermediate energy-density contour of each configuration of the computer-generated system is carried out. The results strongly reinforce the picture of an ensemble of configurations, each consisting of sharply divided liquid and gas regions, but with a highly fluctuating interfacial surface.

2. LONGITUDINAL CORRELATIONS

Our model system consists of 1728 particles, interacting via a classical mechanical Lennard-Jones (6, 12) potential

$$\begin{aligned} \phi(r) &= V(r) - V(r_0), \qquad 0 \leqslant r \leqslant r_0 \\ &= 0, \qquad\qquad\quad r_0 \leqslant r \end{aligned} \tag{1}$$

where $V(r) = 4\epsilon[(\sigma/r)^{12} - (\sigma/r)^6]$ and $r_0 = 2.5\sigma$. We choose σ, ϵ, and $\tau_0 = (m\sigma/48\epsilon)^{1/2}$ as length, energy, and time units (for real argon, $\sigma = 3.405$ Å, $\epsilon = 119.4$°K, and $\tau_0 = 3.112 \times 10^{-13}$ sec). The particles are placed in a fully periodic box of size $L \times L \times 3L$ (with $L = 13.15\sigma$), with a Maxwellian distribution of velocities corresponding to a mean temperature of 0.704 (84°K). The details of creating an inhomogeneous system without any external field in this periodic box, using molecular dynamics, are presented elsewhere.[5]

After the film equilibrates (showing constant temperature and pressure in liquid and gas), the configurations are stored on magnetic tape at intervals of $0.128\tau_0$, and equilibrium quantities computed as averages over 800 configurations, as well as over any theoretical directions of invariance. The full density profile that develops is shown in Fig. 2, consisting of a central liquid third of bulk density $n_0 = 0.76$ and two-thirds vapor of bulk density $n_1 = 0.0033$. Here, interfaces are perpendicular to the long (z) direction.

The shape of the density profile has been the subject of numerous theoretical studies, mainly before reliable numerical knowledge existed. Each of these was compelled to make a critical assumption as to the form of the pair distribution function in the inhomogeneous system. We are now in a position to evaluate the assumptions. Since the mean density variation is only in the longitudinal (z) direction, we first concentrate upon the longitudinal correlations. The two-particle distribution $\rho^{(2)}(\mathbf{r}_1, \mathbf{r}_2)$ denotes the

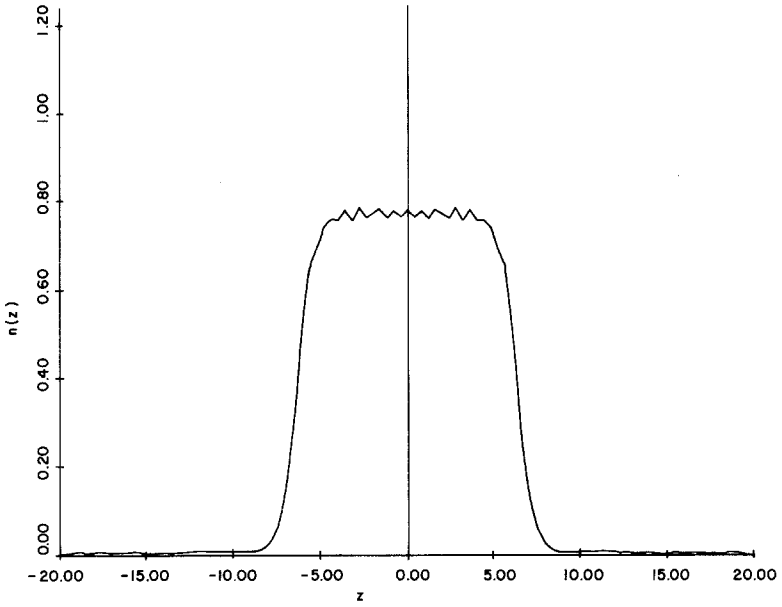

Fig. 2. Full density profile for 84°K model argon in periodic rectangular parallelepiped.

number of distinct pairs of particles per unit volume in $\mathbf{r}_1$ space and unit volume in $\mathbf{r}_2$ space. But our system is constructed to be translation invariant in the x and y directions, so we can write

$$\rho^{(2)}(\mathbf{r}_1, \mathbf{r}_2) = \rho^{(2)}(z_1, z_2; x_1 - x_2, y_1 - y_2) \tag{2}$$

indeed depending only on $[(x_1 - x_2)^2 + (y_1 - y_2)^2]^{1/2}$ for infinite interface cross section. By the longitudinal pair distribution, we now mean correlations perpendicular to the surface, viz.

$$\rho_L^{(2)}(z_1, z_2) \equiv \rho^{(2)}(z_1, z_2; 0, 0) \tag{3}$$

The assumptions made as to the structure of an inhomogeneous fluid of course tend to follow local thermodynamics, mimicking—in the small—successful conceptual aspects of bulk systems. Microscopically, the leading level of structure for a homogeneous component of density n is given by the radial distribution function

$$g(\mathbf{r}_1 - \mathbf{r}_2; n) \equiv \rho^{(2)}(\mathbf{r}_1 - \mathbf{r}_2; n)/n^2 \tag{4}$$

How then is this information to be used to estimate the inhomogeneous $\rho^{(2)}(\mathbf{r}_1, \mathbf{r}_2)$?

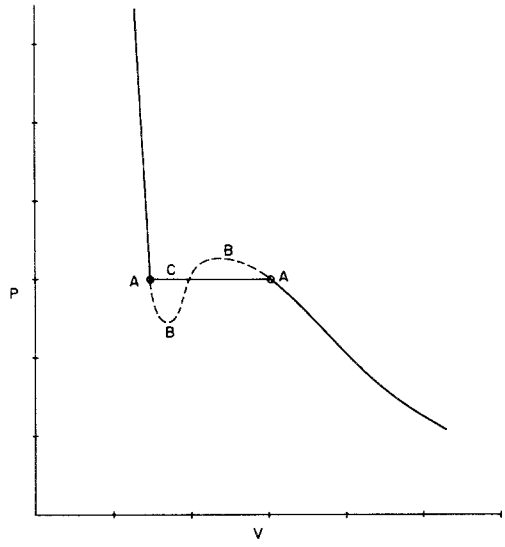

Fig. 3. Typical subcritical isotherm for liquid–vapor transition.

Consider for reference a typical two-phase PV isotherm (Fig. 3). Suppose that an isolated planar two-phase interface is defined—with some suitable recipe—by gas for $z < 0$, liquid for $z > 0$. Then in the zeroth-order Ansatz of Nazarian,[6] one assumes

$$\rho^{(2)}(\mathbf{r}_1, \mathbf{r}_2) = \rho(\mathbf{r}_1)\rho(\mathbf{r}_2)g(\mathbf{r}_1 - \mathbf{r}_2; n) \tag{5}$$

where

$$n = \begin{cases} n_1 \\ n_0 \end{cases} \quad \text{if} \quad \tfrac{1}{2}(z_1 + z_2) \begin{cases} < 0 \\ > 0 \end{cases}$$

effectively restricting consideration to the terminal pure phase points A in Fig. 3, the choice dictated by the center of mass of $\mathbf{r}_1$ and $\mathbf{r}_2$. Toxvaerd[7] avoids the discontinuity in n by choosing n as the center-of-mass density and computing $g(\mathbf{r}_1 - \mathbf{r}_2; n)$ by extrapolation along the metastable–unstable van der Waals loop BB:

$$\rho^{(2)}(\mathbf{r}_1, \mathbf{r}_2) = \rho(\mathbf{r}_1)\rho(\mathbf{r}_2)g(\mathbf{r}_1 - \mathbf{r}_2; \rho[\tfrac{1}{2}(z_1 + z_2)]) \tag{6}$$

To the extent that (6) is a valid starting point, first-order density gradient corrections can be shown to vanish.[8] A third alternative, which we shall examine in some detail, is to move along the two-phase coexistence line C. This requires some explanation.

For the bulk fluid in two-phase coexistence, statistical mechanics as ordinarily practiced (see, e.g., Ref. 9) attaches a probability $p_0 = 1 - p_1$

at each space point for the system to be liquid, and computes all distributions with this weight:

$$\begin{aligned} n &= p_0 n_0 + p_1 n_1 \\ \rho^{(2)}(\mathbf{r}_1 - \mathbf{r}_2) &= p_0 \rho_0^{(2)}(\mathbf{r}_1 - \mathbf{r}_2) + p_1 \rho_1^{(2)}(\mathbf{r}_1 - \mathbf{r}_2) \\ &\text{etc.} \end{aligned} \tag{7}$$

The implication is that gas and liquid are predominantly present only in very large clusters, so that in the course of time a given point—or set of points—can be regarded as either internal to a liquid cluster or internal to a gas cluster. If attention is focused on spatial and temporal regions of transient existence of small clusters, then the interfacial free energy affects the local pressure that can be supported, and the nonnegligible interfacial volume must be averaged into the environment of a given point. This is presumably what (6) takes advantage of. But there is evidence[10] that the structural detail in the vicinity of a rapid density change is very short range and in particular on a scale small compared to that of Fig. 1. Hence a suitable dynamic picture of a two-phase system should indeed include the possibility of an interface sweeping past a given spatial point, but this point can still be regarded as either in gas or in liquid.

The interpretation of the foregoing is clear enough. We can view the two-phase system as a temporal sequence, or phase space ensemble, of configurations each sharply divided into gas and liquid regions. The geometric form of the dividing surface is, however, open. As a primitive approximation, and in accordance with the resulting symmetry, we shall take this as planar. For a given division plane, positioned at Z, we have pure gas for $z < Z$, and pure liquid uncorrelated with gas for $z > Z$. It follows that

$$\begin{aligned} \rho_Z(r) &= n_0 \epsilon(z - Z) + n_1 \epsilon(Z - z) \\ \rho_Z^{(2)}(r_1, r_2) &= n_0^2 g_0(r_1 - r_2)\epsilon(z_1 - Z)\epsilon(z_2 - Z) \\ &\quad + n_0 n_1 [1 - \epsilon(z_1 - Z)\epsilon(z_2 - Z) - \epsilon(Z - z_1)\epsilon(Z - z_2)] \\ &\quad + n_1^2 g_1(r_1 - r_2)\epsilon(Z - z_1)\epsilon(Z - z_2) \end{aligned} \tag{8}$$

where $\epsilon(x)$ is the Heaviside step function, i.e., $[1 + \text{sgn}(x)]/2$. Now if Z is distributed with probability density $f(Z)$ and corresponding cumulative $F(Z) = \int_{-\infty}^{Z} f(Z')\, dZ'$, we have on integration

$$\begin{aligned} \rho(r) &= \int \rho_Z(r) f(Z)\, dZ \\ &= n_0 F(z) + n_1 [1 - F(z)] \\ \rho^{(2)}(r_1, r_2) &= n_0^2 g_0(r_1 - r_2) F(\text{Min}(z_1, z_2)) \\ &\quad + n_0 n_1 [F(\text{Max}(z_1, z_2)) - F(\text{Min}(z_1, z_2))] \\ &\quad + n_1^2 g_1(r_1 - r_2)[1 - F(\text{Max}(z_1, z_2))] \end{aligned} \tag{9}$$

The desired relation between $\rho^{(2)}(r_1, r_2)$ and $\rho(r)$ results from (9) on eliminating the function $F(z)$:

$$\begin{aligned}\rho^{(2)}(r_1, r_2) = {} & [n_0^2/(n_0 - n_1)][\rho(\mathrm{Min}(z_1, z_2)) - n_1]g_0(r_1 - r_2) \\ & + [n_0 n_1/(n_0 - n_1)][\rho(\mathrm{Max}(z_1, z_2)) - \rho(\mathrm{Min}(z_1, z_2))] \\ & + [n_1^2/(n_0 - n_1)][n_0 - \rho(\mathrm{Max}(z_1, z_2))]g_1(r_1 - r_2) \qquad (10)\end{aligned}$$

quite different in form from (5) and (6). However, if n_1 can be neglected, as is the case with our data, (10) reduces to

$$\rho^{(2)}(r_1, r_2) = n_0\rho(\mathrm{Min}(z_1, z_2))g_0(r_1 - r_2) \qquad (10')$$

very much in the same mold as (5) and (6). The radial distribution function at liquid density to serve as input to (10′) is shown in Fig. 4.

We can now return to the question of longitudinal correlations. According to (10′), we should have

$$\rho_L^{(2)}(z_1, z_2) = n_0\rho_{\min}g_0(\Delta z) \qquad (11)$$

and so the ratio $\rho_L^{(2)}/n_0\rho_{\min}$ has been plotted in Fig. 5 for several values of $\Delta z \equiv z_1 - z_2$, as a function of $\bar{z} = (z_1 + z_2)/2$. Although the computer values of $\rho_L^{(2)}$ vary by a factor of 50 in the range examined, this ratio remains very nearly constant—and with correct constant—at each fixed value of Δz.

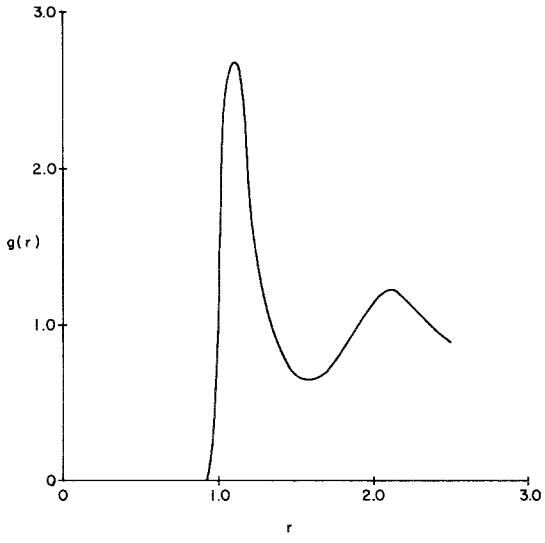

Fig. 4. Radial distribution function $g_0(r)$ for 84°K model argon at liquid density $n_0 = 0.76$.

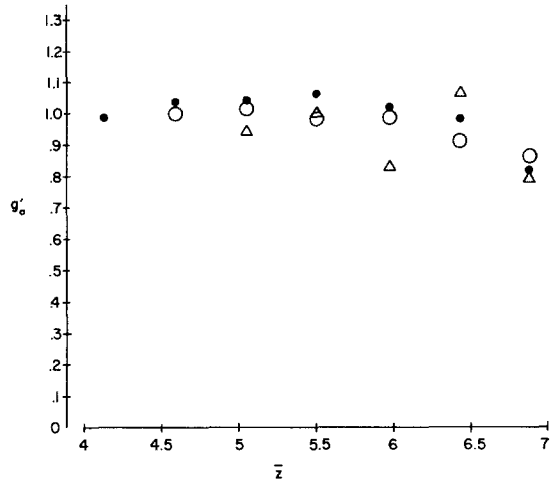

Fig. 5. $g_0'(\bar{z}, \Delta z) \equiv \rho_L^{(2)}(z_1, z_2)/n_0\rho_{\min}(z)$ as a function of $\bar{z} \equiv (z_1 + z_2)/2$ at fixed $\Delta z \equiv z_1 - z_2$. Solid circles denote $\Delta z = 1.38$, open circles $\Delta z = 2.31$, open triangles $\Delta z = 3.23$.

We conclude that the approximation represented by an ensemble average of sharply separated gas–liquid regions, even with the further assumption of a strictly planar interface, provides an adequate picture of longitudinal correlations in our model system with its model parameters. A similar test of (6) requires much more bulk system input data and is correspondingly less definitive; an approximate check did not lead to substantially poorer results in the region examined. The advantage of (10) and (10′) is their greater simplicity and deeper dynamical implications. In addition, they can be easily improved. We will pursue these advantages.

3. THE DENSITY PROFILE

The conventional way of using information on $\rho^{(2)}$ to obtain an interphase density profile has been to insert this into an exact relation connecting $\rho^{(2)}$ and ρ. For this purpose, the first of the BBGKY hierarchy (local balance of mechanical and thermodynamic forces)

$$\nabla\rho(r) + \beta \int \rho^{(2)}(r, r')\, \nabla\phi(r - r')\, d^3r' = 0 \tag{12}$$

with ϕ the pair interaction, has generally—but not universally[11]—been employed. The qualitative nature of the profiles is easily established. We consider any region in which $\rho(r)$ is close to the bulk fluid (gas or liquid)

density n, and, using (5) or (6), set $\rho^{(2)}(r, r') = \rho(r)\rho(r')g(r - r')$, where g is referred to density n. For a plane symmetric profile $\rho(z)$, (12) becomes

$$\rho'(z) = -\beta\rho(z) \int g(r')(z'/r')\phi'(r')\rho(z - z')\, d^3r' \tag{13}$$

Assuming $g\phi'$ short range on the scale of ρ, we can Taylor-expand $\rho(z - z')$ about z, so that, on using the nonvanishing angular averages $\langle z'^{2s} \rangle = r'^{2s}/(2s + 1)$, we have

$$\begin{aligned} \rho'(z) = -\beta\rho(z) \int & g(r')\phi'(r') \\ & \times [-\tfrac{1}{3}r'\rho'(z) - (1/30)r'^3\rho'''(z) + \cdots]\, d^3r' \end{aligned} \tag{14}$$

Hence, inserting the virial pressure,

$$\rho'(z) = a\rho'(z) + b\rho(z)\rho'''(z) + \cdots \tag{14'}$$

where

$$a = 2(n - \beta P)/n^2$$

$$b = (\beta/30) \int g(r')r'\phi'(r')r'^2\, d^3r'$$

To solve (14'), we need only integrate, obtaining

$$\rho(z) = K + 0.5a\rho(z)^2 + 0.5b[2\rho(z)\rho''(z) - \rho'(z)^2] \tag{15}$$

for suitable K. Now multiply by $\rho'(z)/\rho(z)^2$ and integrate, yielding

$$K' + \ln \rho(z) = -K/\rho(z) + 0.5a\rho(z) + 0.5b\rho'(z)^2/\rho(z) \tag{15'}$$

for suitable K'. If $\rho(z) = n$ is to satisfy (15) and (15'), K and K' are determined, allowing (15') to be written as

$$\begin{aligned} n^2b[\rho'(z)/n]^2 = {} & 2\rho(z)\{\ln[\rho(z)/n] - 1 + n/\rho(z)\} \\ & - n^2a[\rho(z)/n - 1]^2 \end{aligned} \tag{16}$$

Finally, expanding in small $\Delta(z) \equiv \rho(z)/n - 1$,

$$n^2b[\Delta'(z)]^2 = (2\beta P - n)\,\Delta(z)^2 \tag{16'}$$

Working in from gas and liquid ends, this results in exponential deviations into the interface region, with a much more rapid *relative* rise from the low-n gas side (see Fig. 6). It is then the nature of the connection region that distinguishes, e.g., (5) from (6).

The need for simultaneous knowledge of ϕ and g is more than a small inconvenience if one wants ultimately to make use of experimental data. However, one can always write down a $\rho^{(2)}$–ρ relation in which the internal

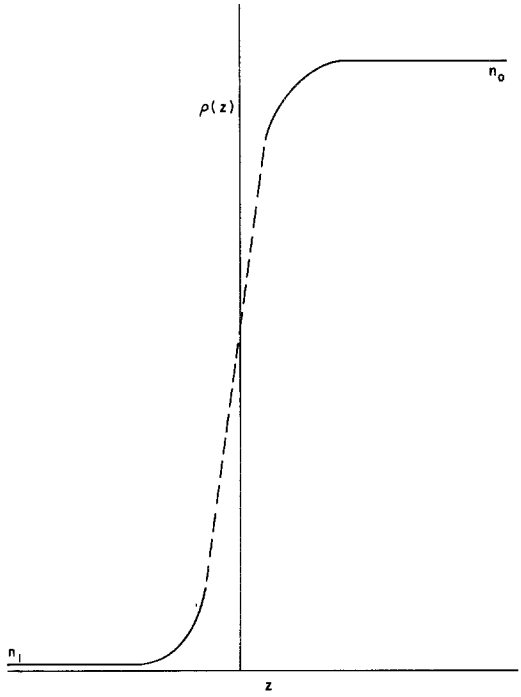

Fig. 6. Density profile from Eq. (16).

potential ϕ does not appear at all. This is most easily derived by putting the system in an external field $u(r)$. It is known[8] that at fixed chemical potential, a change in u produces a change in ρ according to the linear response relation

$$\delta\rho(r) = -\beta \int [\rho^{(2)}(\mathbf{r}, \mathbf{r}') + \rho(\mathbf{r})\,\delta(\mathbf{r} - \mathbf{r}') - \rho(r)\rho(r')]\,\delta u(\mathbf{r}')\,d^3r'$$

$$\equiv -\beta \int S^{(2)}(\mathbf{r}, \mathbf{r}')\,\delta u(\mathbf{r}')\,d^3r' \tag{17}$$

or its inverse

$$-\beta\,\delta u(r) = \int C^{(2)}(\mathbf{r}, \mathbf{r}')\,\delta\rho(\mathbf{r}')\,d^3r' \tag{17'}$$

Here

$$C^{(2)}(\mathbf{r}, \mathbf{r}') = \delta(\mathbf{r} - \mathbf{r}')/\rho(\mathbf{r}) - c(\mathbf{r}, \mathbf{r}') \tag{18}$$

where $c(\mathbf{r}, \mathbf{r}')$ is the usual direct correlation function. For a translation-

invariant internal potential, a unit translation of the whole system produces[12] $\delta u(\mathbf{r}) = \nabla u(\mathbf{r})$, $\delta\rho(\mathbf{r}) = \nabla\rho(\mathbf{r})$, whence

$$-\beta\,\nabla u(\mathbf{r}) = \int C^{(2)}(\mathbf{r}, \mathbf{r}')\,\nabla\rho(\mathbf{r}')\,d^3r' \tag{19}$$

Now if $u(\mathbf{r}) = 0$, one has the desired result[13–15]

$$\nabla\rho(\mathbf{r}) = \rho(\mathbf{r}) \int c(\mathbf{r}, \mathbf{r}')\,\nabla\rho(\mathbf{r}')\,d^3r' \tag{20}$$

Approximations inserted into (20) may of course give dramatically different results than when inserted into (12). But the most convenient approximations are in fact those for c (Ref. 15) and not for $\rho^{(2)}$. The analogs of (4) or (6) have not yet been used for this purpose, and indeed the function c would be expected to become singular at infinite compressibility in the metastable region. However, the wings of the interphase region can presumably be analyzed as was (12). We expand the plane symmetric case, obtaining for $c(\mathbf{r}, \mathbf{r}') = c(\mathbf{r} - \mathbf{r}')$

$$\begin{aligned}\rho'(z) &= \rho(z) \int c(r')\rho'(z - z')\,d^3r' \\ &= \rho(z)[A\rho'(z) + B\rho'''(z)]\end{aligned} \tag{21}$$

where

$$A = \int c(r')\,d^3r' = \frac{1}{n}\left(1 - \frac{\partial\beta P}{\partial n}\right)$$

$$B = \tfrac{1}{6}\int r'^2 c(r')\,d^3r'$$

and conclude that

$$nB[\Delta'(z)]^2 = \frac{\partial\beta P}{\partial n}\,\Delta(z)^2 \tag{21'}$$

which has the same character as (16′). The exponent $K = (\partial\beta P/nB\,\partial n)^{1/2}$ associated with the exponential falloff of Δ in (21′) represents an inverse correlation length, and has appeared repeatedly in the literature dating back to Ornstein and Zernike.

There is of course no point to using a $\rho^{(2)}$–ρ relation more accurate than the approximation to $\rho^{(2)}$, *if* the same mechanism is responsible for the inaccuracy of each. The approximation (10) was based upon neglect of the gas–liquid interaction and the associated longitudinal fine structure, so that for each configuration of the relevant ensemble, each volume element either

belongs to liquid at density n_0 or gas at density n_1. Suppose that we have some microscopic criterion in the form of an observable $Q(\mathbf{r}_1,\ldots,\mathbf{r}_N;\mathbf{r})$, so that

$$\begin{aligned} Q(\mathbf{r}) &> 0 \quad \text{implies} \quad \text{liquid at } \mathbf{r} \\ Q(\mathbf{r}) &< 0 \quad \text{implies} \quad \text{gas at } \mathbf{r} \end{aligned} \tag{22}$$

Then the mean density at $\mathbf{r}$ under the above assumption becomes simply

$$\begin{aligned} \rho(\mathbf{r}) &= n_0\langle\epsilon(Q(\mathbf{r}))\rangle + n_1\langle\epsilon(-Q(\mathbf{r}))\rangle \\ &= 0.5(n_0 + n_1) + 0.5(n_0 - n_1)\langle\operatorname{sgn}(Q(\mathbf{r}))\rangle \end{aligned} \tag{23}$$

Now

$$\begin{aligned} \langle\operatorname{sgn} Q(\mathbf{r})\rangle &= \frac{1}{\pi i} P\int \langle\exp[isQ(\mathbf{r})]\rangle \frac{ds}{s} \\ &\approx \frac{1}{\pi i} P\int \exp[is\bar{Q}(\mathbf{r}) - s^2\sigma^2(\mathbf{r})]\frac{ds}{s} \end{aligned} \tag{24}$$

to second cumulant order, where

$$\bar{Q}(\mathbf{r}) = \langle Q(\mathbf{r})\rangle, \qquad \sigma^2(\mathbf{r}) = \langle Q^2(\mathbf{r})\rangle - \langle Q(\mathbf{r})\rangle^2 \tag{24'}$$

Evaluating (by applying $\partial/\partial Q$), we have

$$\rho(\mathbf{r}) = n_1 + \frac{n_0 - n_1}{(2\pi)^{1/2}}\int_{-\infty}^{\bar{Q}(r)/\sigma(r)} e^{-t^2/2}\,dt \tag{25}$$

For plane symmetry, ρ, $\bar{Q}$, and σ are functions of z alone. Suppose that the mean interface is at $z = 0$, i.e., $\bar{Q}(0) = 0$. Then, to leading order in z, we have the error function representation

$$\rho(z) = n_1 + \frac{n_0 - n_1}{(2\pi)^{1/2}}\int_{-\infty}^{z/\lambda} e^{-t^2/2}\,dt \tag{26}$$

where $\lambda = \sigma(0)/\bar{Q}'(0)$. But what shall we choose as $Q(\mathbf{r})$? In order to make use of one- and two-body data, Q must contain only zero- and one-body terms, and of course be invariant to translation of z and of the whole system. Thus

$$Q(\mathbf{r}) = \sum_i \tau(\mathbf{r}_i - \mathbf{r}) - \tau_0 \tag{27}$$

Since $\bar{Q}(0) = 0$, we have $\tau_0 = \int \rho(z')\tau(\mathbf{r}')\,d^3r'$, and so the parameters of (24') become

$$\begin{aligned} \bar{Q}(z) &= \int [\rho(z' + z) - \rho(z')]\tau(\mathbf{r}')\,d^3r' \\ \sigma^2(z) &= \int\int S^{(2)}(\mathbf{r}', \mathbf{r}'')\tau(\mathbf{r}' - z)\tau(\mathbf{r}'' - z)\,d^3r'\,d^3r'' \end{aligned} \tag{28}$$

In particular

$$\begin{aligned} \bar{Q}'(0) &= 0 \\ \sigma^2(0) &= \int\int S^2(\mathbf{r}', \mathbf{r}'')\tau(\mathbf{r}')\tau(\mathbf{r}'')\, d^3r'\, d^3r'' \end{aligned} \tag{28'}$$

In the numerical case under discussion, the gas density n_1 is very low. Let us choose $n_1 = 0$, so that (10′) applies. After some manipulation, the distance parameter λ of (26) then takes the form

$$\begin{aligned} \lambda^2 = \Bigg\{ &\int\int [\rho(z_{\min})S_0^{(2)}(\mathbf{r} - \mathbf{r}')\tau(\mathbf{r})\tau(\mathbf{r}')/n_0]\, d^3r\, d^3r' \\ &+ \int\int [n_0 - \rho(z_{\max})]\rho(z_{\min})\tau(\mathbf{r})\tau(\mathbf{r}') \Bigg\} \Bigg[\int \rho'(z)\tau(\mathbf{r})\, d^3r \Bigg]^{-2} \end{aligned} \tag{29}$$

and our task is to solve this for λ.

Assuming that the range of $S_0^{(2)}$ is small on the scale of interest, we shall make the replacement

$$\begin{aligned} S_0(\mathbf{r} - \mathbf{r}') &\to \int S_0^{(2)}(\mathbf{r}'')\, d^3r''\, \delta(\mathbf{r} - \mathbf{r}') \\ &= n_0(\partial n_0/\partial\beta P)\, \delta(\mathbf{r} - \mathbf{r}') \end{aligned}$$

in Eq. (29). Finally, there is the question of the choice of the density test function τ, although the results should not be sensitive to this choice. We shall take τ as Gaussian:

$$\tau(\mathbf{r}) = \tau(x)\tau(y)\tau(z) = \frac{1}{(2\pi)^{3/2}U^3} \exp\left[-\frac{r^2}{2U^2}\right] \tag{30}$$

so that $Q(\mathbf{r})$ is indeed a measure of the local density at $\mathbf{r}$. Now (29) can be written as

$$\begin{aligned} \lambda^2 \Bigg[\int \rho'(z)\tau(z)\, dz \Bigg]^2 = \kappa n_0 &\int \rho(z)\tau(z)^2\, dz \Bigg[\int \tau(z)^2\, dz \Bigg]^2 \\ &+ \iint\limits_{z+z'<0} \rho(z)\rho(z')\tau(z)\tau(z')\, dz\, dz' \end{aligned} \tag{31}$$

where $\kappa = (1/n_0)\, \partial n_0/\partial\beta P$ denotes the compressibility. After a somewhat tedious evaluation, (31) attains the form

$$\lambda^3 = \pi^{3/2}\kappa/[2F(x)]$$

where

$$\begin{aligned} F(x) &= x^3\{[4\pi^2/(1 + x^2)] - x^2[\tfrac{1}{4}\pi + \tan^{-1} x/(2 + x^2)^{1/2}]\} \\ x &= \nu/\lambda \end{aligned} \tag{32}$$

To make sure that λ is insensitive to the value of ν, we demand that $F'(x) = 0$, resulting in the numerical value $F(x) = 34$ at $x = \nu/\lambda = 1.6$. Hence

$$\lambda \sim 0.44\kappa^{1/3} \qquad \text{or} \qquad \rho'(0) \sim n_0/[(2\pi)^{1/2}\lambda] = 0.92 n_0 \kappa^{-1/3} \tag{33}$$

This approximation should be appropriate to the center of the interface region rather than the wings. Using the measured value $\kappa = 0.04$, we find, from (33), $\rho'(0) \sim 2.1$. On the other hand, the measured density profile is much broader, with $\rho'(0) \sim 0.35$ at the half-density point in the interface. We shall soon see why this is the case.

4. TRANSVERSE CORRELATIONS

Neither version (6) nor (10) of local thermodynamics appears to show major qualitative deficiencies when longitudinal effects, be they density profile or density correlations, are in question. The situation deteriorates rapidly but informatively when transverse correlations are considered. For pure transverse correlations, we identify the z values of the points in question, and thus define the transverse pair distribution (for correlations parallel to the surface) by

$$\rho_T^{(2)}(z, \mathbf{r}_{12}) \equiv \rho^{(2)}(x_1, y_1, z, x_2, y_2, z) \tag{34}$$

where $\mathbf{r}_{12} = (x_1 - x_2, y_1 - y_2)$. According to approximation (6),

$$\rho_T^{(2)}(z, \mathbf{r}_{12}) \simeq \rho(z)^2 g(\mathbf{r}_{12}; \rho(z)) \tag{35}$$

while, according to (10),

$$\rho_T^{(2)}(z, \mathbf{r}_{12}) \simeq \frac{\rho(z) - n_1}{n_0 - n_1} n_0^2 g_0(\mathbf{r}_{12}) + \frac{n_0 - \rho(z)}{n_0 - n_1} n_1^2 g_1(\mathbf{r}_{12}) \tag{36}$$

The corresponding approximations for the transverse correlation function $F_T^{(2)}(z, \mathbf{r}_{12}) = \rho_T^{(2)}(z, \mathbf{r}_{12}) - \rho(z)^2$ then become

$$F_T^{(2)}(z, \mathbf{r}_{12}) \simeq F^{(2)}(\mathbf{r}_{12}; \rho(z)) \tag{37}$$

$$F_T^{(2)}(z, \mathbf{r}_{12}) \simeq \frac{\rho(z) - n_1}{n_0 - n_1} F_0^{(2)}(\mathbf{r}_{12}) + \frac{n_0 - \rho(z)}{n_0 - n_1} F_1^{(2)}(\mathbf{r}_{12}) + [n_0 - \rho(z)][\rho(z) - n_1] \tag{38}$$

It is convenient to go over to transverse Fourier space:

$$F_T(z, \mathbf{k}) \equiv \frac{1}{\rho(z)} \int F_T^{(2)}(z, \mathbf{r}_{12}) \exp(i\mathbf{k}\cdot\mathbf{r}_{12})\, d^2 r_{12} \tag{39}$$

While (37) and (38) evoke similar behavior in $F_T(z, \mathbf{k})$ for $\mathbf{k} \neq 0$, i.e., a bulk $F(k)$ at some mean density compared to a mean of $F_0(\mathbf{k})$ and $F_1(\mathbf{k})$, the behavior at $\mathbf{k} = 0$ is qualitatively different: regular for (37), but singular for (38). How do these compare with our numerical simulation? In the simulation, we compute

$$\bar{S}_T(z, \mathbf{k}) = \left\langle \sum_{i,j=1}^{N(\Delta z)} \exp[-i\mathbf{k}\cdot(\mathbf{r}_1 - \mathbf{r}_2)] \right\rangle \Big/ \langle N(\Delta z) \rangle \tag{40}$$

where $\mathbf{k} = (2\pi n/L, 2\pi m/L, 0)$, $m, n = 0, 1, 2,...$; $mn \neq 0$, i and j running over the $N(\Delta z)$ atoms in a slice of volume $L \times L \times \Delta z$ centered at z. The angular brackets denote the average over all configurations, and common values of k^2 are averaged as well. For small Δz, it is easy to see that

$$\bar{S}_T(z, \mathbf{k}) = 1 + F_T(z, \mathbf{k})\, \Delta z \tag{40'}$$

In Figs. 7 and 8, $\bar{S}_T(z, \mathbf{k})$ is plotted as a function of k for two values of z: in the middle of the bulk liquid and in the middle of the interface. In Fig. 8, the circles show $\bar{S}_T(k)$ calculated with 1024 particles in a box of size $6.78\sigma \times 6.78\sigma \times 56.24\sigma$. The close agreement down to the smallest k of the smaller system lends credence to the reliability of the numerical results.

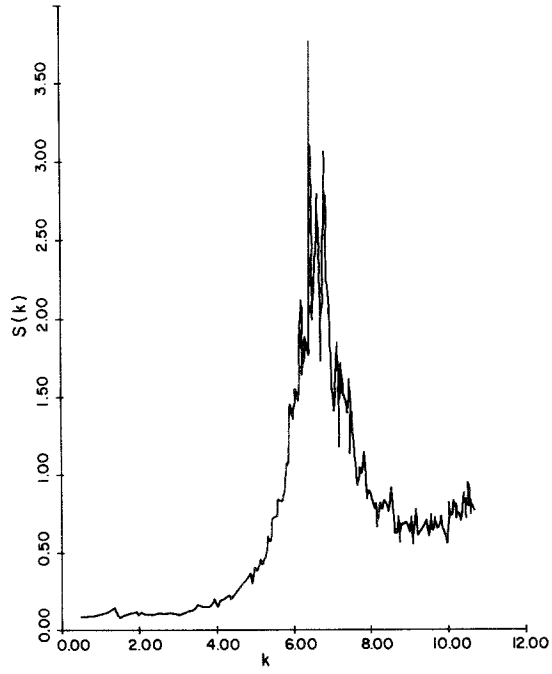

Fig. 7. The k dependence of the transverse structure factor in liquid, $z = 0$.

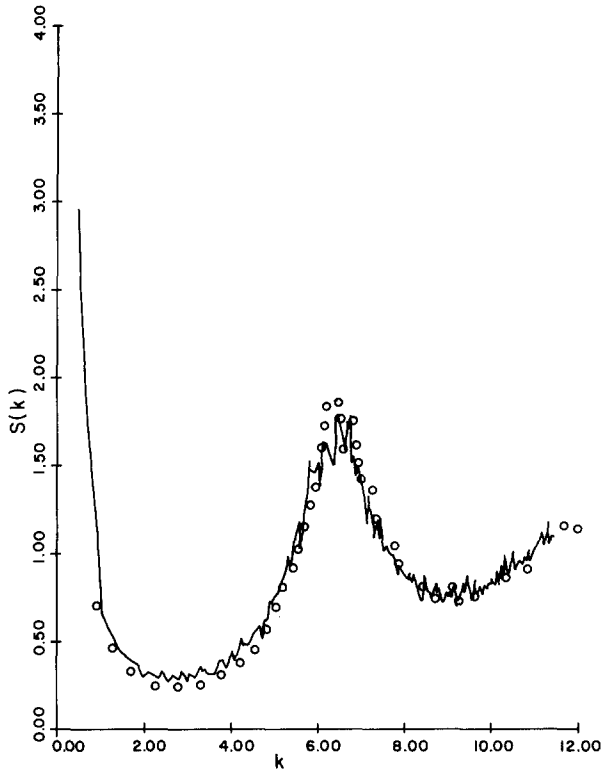

Fig. 8. The k dependence of the transverse structure factor at mid-interface, $z = 7.5$. Curve shows system of 1728 particles, the circles denote system of 1024 particles.

The enhancement of low-k values in the interface region is brought out strikingly in Fig. 8. There is apparent divergence as $k \to 0$, indicating transverse correlations over the size of the box. One can say that the totally correlated $k = 0$ component of (38) is in reality smeared into a merely very long-range correlation. To bring out the contrast, we plot in Fig. 9 the difference between $\bar{S}_T$ obtained from simulation and that predicted by (38), for the minimum value of k. This difference is indeed confined to the interface region, and closely resembles the curve of $\rho'(z)^2$, also drawn. We will comment on this relation in a moment. Lack of reliable knowledge of the predictions of (37) precludes a similar comparison. But we can say in general that its extrapolation from physical (one-phase) densities will certainly not introduce the observed singular k behavior. On the other hand, an independent assessment of the metastable state correlations should at least exhibit a divergence as $k \to 0$ at the points of infinite compressibility.

The genesis of singular low-k transverse behavior has been suggested

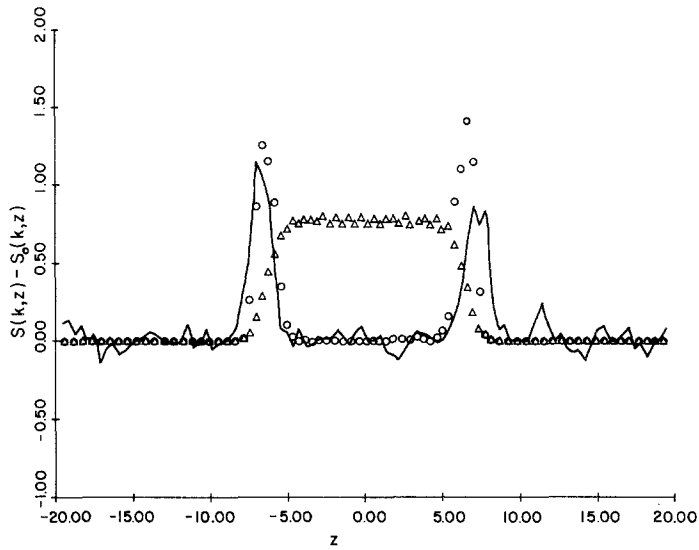

Fig. 9. The z dependence of excess transverse structure factor at $k = 2\pi/13.15$, $\Delta z = 0.4$ (line); $\rho(z)$ is shown by triangles. Comparison curve of $10\rho\,(z)^2$ shown by circles.

in a recent paper of Wertheim.[15] A brief step beyond his analysis is all that we require. Suppose that we take the transverse Fourier transforms of $C^{(2)}$ and $S^{(2)}$, denoting these by C and S. Then [see (17), (17′)]

$$\int C(z_1, z_2; \mathbf{k}) S(z_2, z_3; \mathbf{k})\, dz_2 = \delta(z_1 - z_2) \tag{41}$$

so that $C(k)$ and $S(k)$ are again inverse matrices. On the other hand, according to (19) and (20) in the plane symmetric case,

$$\int C^{(2)}(z_1, z_2; \mathbf{r}_{12}) \rho'(z_2)\, d^3 r_2 = 0 \tag{42}$$

or

$$\int C(z_1, z_2; 0) \rho'(z_2)\, dz_2 = 0 \tag{42'}$$

Thus $C(0)$ has $\rho'(z)$ as a zero-eigenvalue eigenfunction, and does not have an inverse. But if $C(k)$ is a function of k^2 alone, analytic in k^2 around $k^2 = 0$, we can certainly write

$$C(z_1, z_2; \mathbf{k}) = C(z_1, z_2) + k^2 C'(z_1, z_2) + \cdots \tag{43}$$

where

$$C'(z_1, z_2) = \tfrac{1}{4} \int C^{(2)}(z_1, z_2; \mathbf{r}_{12}) r_{12}^2\, d^2 r_{12}$$

In a representation including the $C(0)$ eigenfunction

$$\psi_0(z) = \rho'(z)/\left\{\int [\rho'(z)]^2\, dz\right\}^{1/2} \tag{44}$$

(assumed nondegenerate), the only small diagonal element of $C(k)$ is

$$C_{00}(k) = k^2\left[\int \rho'(z_1)C'(z_1, z_2)\rho'(z_2)\, dz_1\, dz_2\right]\left[\int \rho'(z)^2\, dz\right]^{-1} \tag{44'}$$

Thus (readily verified by standard perturbation theory) the only singular element of $S(k)$ is $S_{00}(k) = 1/C_{00}(k)$ and we have

$$S(z_1, z_2; k) = \frac{1}{k^2}\frac{\rho'(z_1)\rho'(z_2)}{\int \rho'(z)C'(z_1, z_2)\rho'(z_2)\, dz_1\, dz_2} + \cdots \tag{45}$$

together with nonsingular terms in k.

The $\rho'(z)^2/\rho(z)$ dependence of $F_T(z, \mathbf{k})$, as defined by (39), is indeed that observed in Fig. 8. Only the magnitude of the singularity remains to be discussed. But in fact the surface tension can be written[13] as

$$\gamma = \frac{1}{4\beta}\int \rho'(z_1)r_{12}^2 C^{(2)}(z_1, z_2; \mathbf{r}_{12})\rho'(z_2)\, dz_1\, dz_2\, d^2r_{12} \tag{46}$$

We conclude, on identifying the deviation from a plane interface ensemble with the singular part (45), that to leading order in k,

$$F_T(z, \mathbf{k}) = \frac{1}{\beta\gamma}\frac{1}{k^2}\frac{\rho'(z)^2}{\rho(z)} \tag{47}$$

In the present case, $\beta = 1/0.7$, $\gamma = 0.7$, $\rho(z) = 0.35$. If the choice $\rho'(z) = 0.50$ is made, well within the margin of error, the simulated F_T, from (40') falls quite well on the curve (47) (see Fig. 10). The coefficient is not very precise, but the $1/k^2$ shape is well established.

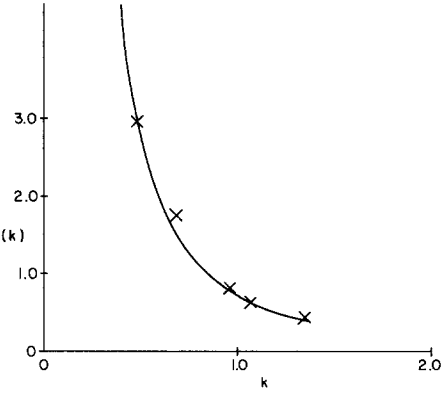

Fig. 10. Low-k transverse correlations at mid-interface. Solid curve from Eq. (47), computer simulation points denoted by crosses.

Equation (45) was derived on quite general grounds of consistency, but its form is quite suggestive of a physical mechanism. The point is this. According to (38), there is a δ-function singularity in $F_T(z, \mathbf{k})$ at $\mathbf{k} = 0$. The basis of this is the assumption of a plane interface between liquid and vapor. This assumption of perfect coherence is most unphysical for large separation in the interface, and we expect some weaker small-k behavior. Indeed, in the absence of infinite-range correlations, one must have the asymptotic results

$$\begin{aligned} \rho^{(2)}(\mathbf{r}_1, \mathbf{r}_2) &\to \rho(z_1)\rho(z_2) \\ F_T^{(2)}(z, \mathbf{r}_{12}) &\to 1 \end{aligned} \tag{48}$$

as $|\mathbf{r}_1 - \mathbf{r}_2| \to \infty$ or $\mathbf{r}_{12} \to \infty$, respectively. These are of course consistent with (6). Thus, although the local z profile may be represented by (10), global structure is not. But the amplitude of the deviation goes as kT/γ, strong evidence that one is looking at modes thermally excited against surface tension. Surface modes[16–18] are clearly the leading candidates.

It is tempting then to build up the true surface configuration by "unfreezing" surface modes on a bare or intrinsic surface profile. This, however, requires firm knowledge of mode–mode correlations and hence may not be useful for detailed questions about surface structure. If instead one looks at infinitesimal changes in surface mode amplitudes, the objection does not hold. Indeed, pair correlations can be assessed in this fashion. $S^{(2)}(\mathbf{r}, \mathbf{r}')$ in a classical fluid serves not only as density–density correlation, but also [see (17)] as linear response to an infinitesimal applied field. Suppose then that an external potential $u(r)$ is applied, resulting in a distortion of the $z = 0$ surface of amplitude $\xi(\mathbf{x}) \equiv \xi(x, y)$. In other words, the new density profile is

$$\begin{aligned} \rho_\xi(\mathbf{r}) &= \rho(z - \xi(\mathbf{x})) \\ \xi(\mathbf{x}) &= \frac{1}{L^2} \sum_k \xi_\mathbf{k} \exp(-i\mathbf{k}\cdot\mathbf{x}) \end{aligned} \tag{49}$$

Now—at least at long wavelength—a surface tension γ implies a surface energy of $E = \gamma \int (1 + |\nabla\xi|^2)^{1/2}\, d^2x$. Hence the energy change through second order in u and ξ is

$$\begin{aligned} \Delta E &= (\gamma/2) \int |\nabla\xi|^2\, d^2x + \int [\rho(z) - \xi(\mathbf{x})\rho'(z)]u(r)\, d^3r \\ &= (\gamma/2)(1/L^2) \sum k^2 \xi_\mathbf{k}\xi_{-\mathbf{k}} + \int \rho(z)u(\mathbf{r})\, d^3r \\ &\quad - (1/L^2) \int \sum \xi_\mathbf{k}\rho'(z)u(\mathbf{r}) \exp(-i\mathbf{k}\cdot\mathbf{x})\, d^3r \end{aligned} \tag{50}$$

Using the Boltzmann weight $e^{-\beta \Delta E}$, the free energy change associated with (50) becomes

$$\Delta F(u) = \int \rho(z)u(r)\, d^3r - (1/2L^2) \sum \left| \int \rho'(z)u(\mathbf{r}) \exp(-i\mathbf{k}\cdot\mathbf{z})\, d^3r \right|^2 /\gamma k^2 \tag{51}$$

But $\Delta\rho(r\,|\,u) = \delta\Delta F(u)/\delta u(\mathbf{r})$, and $S(\mathbf{r}, \mathbf{r}') = -\delta\Delta\rho(\mathbf{r}\,|\,u)/\delta\beta u(\mathbf{r}')$. It follows that at long wavelength

$$S(\mathbf{r}, \mathbf{r}) = (1/\beta\gamma L^2)\{\rho'(z)\rho'(z') \exp[-i\mathbf{k}\cdot(\mathbf{x} - \mathbf{x}')]\}/k^2 \tag{52}$$

and hence

$$F_T(z, k) = \rho'(z)^2/[\beta\gamma k^2 \rho(z)] \tag{52'}$$

exactly reproducing (47).

When is it reasonable to examine not just infinitesimal changes in ξ but rather the full amplitude of surface waves in the bare interface alluded to above? Perhaps if only a one-particle property such as the density profile itself is in question. Suppose then that $\rho_0(z) = n_0\epsilon(z)$ denotes the idealized bare density profile, γ_0 the corresponding surface tension, and $\xi(\mathbf{x})$ the full microscopic surface distortion. We then have

$$\rho(z) = \langle \rho_\xi(\mathbf{r}) \rangle = n_0 \langle \epsilon(z - \xi(\mathbf{x})) \rangle \tag{53}$$

or

$$\rho'(z) = \frac{n_0}{2\pi} \int \exp\{is[z - \xi(\mathbf{x})]\}\, ds \tag{54}$$

According to (50), at $u = 0$,

$$\langle e^{-is\xi} \rangle = \left\langle \exp\left[-(is/L^2) \sum \xi_\kappa \exp(-i\mathbf{k}\cdot\mathbf{z}) \right] \right\rangle$$

$$= \exp\left[-\tfrac{1}{2}(s^2/\beta\gamma_0 L^2) \sum (1/k^2) \right]$$

Hence

$$\rho'(z) = \frac{n_0}{(2\pi)^{1/2}\lambda} \exp\left[-\frac{z^2}{2\lambda^2} \right] \tag{55}$$

where

$$\lambda^2 = \frac{1}{\beta\gamma_0 L^2} \sum \frac{1}{k^2} \quad (= \langle \xi^2 \rangle) \tag{55'}$$

The $k = 0$ term in (55') cannot of course be present in the form shown. As we have previously discussed, the motion implied must have a short coherence length and presumably gives rise to that portion of λ^2 represented by (33). The remainder of the sum in (55') is not small. In fact, it would diverge at large (two-dimensional) k if not cut off at some characteristic

length a_0, e.g., interparticle spacing, or width of density profile.[16] Writing $\mathbf{k} = (2\pi/L)(K_1, K_2)$ for integer K_1, K_2, setting $K_{\max} = (2\pi/a_0)/(2\pi/L) = L/a_0$, and approximating the sum in (55′) by an integral, we have

$$\lambda^2 = \lambda_0^2 + \frac{\ln(L/a_0)}{2\pi\beta\gamma_0} \tag{56}$$

where λ_0^2 is the $\mathbf{k} = 0$ contribution. Thus the "capillary waves" $\mathbf{k} \neq 0$ make a large (and it seems ultimately divergent) contribution to the broadening of the density profile.

5. SURFACE DYNAMICS

We have been led to a picture of the phase transition region in which a quasiplane symmetric pattern of parallel surface motions of relatively short

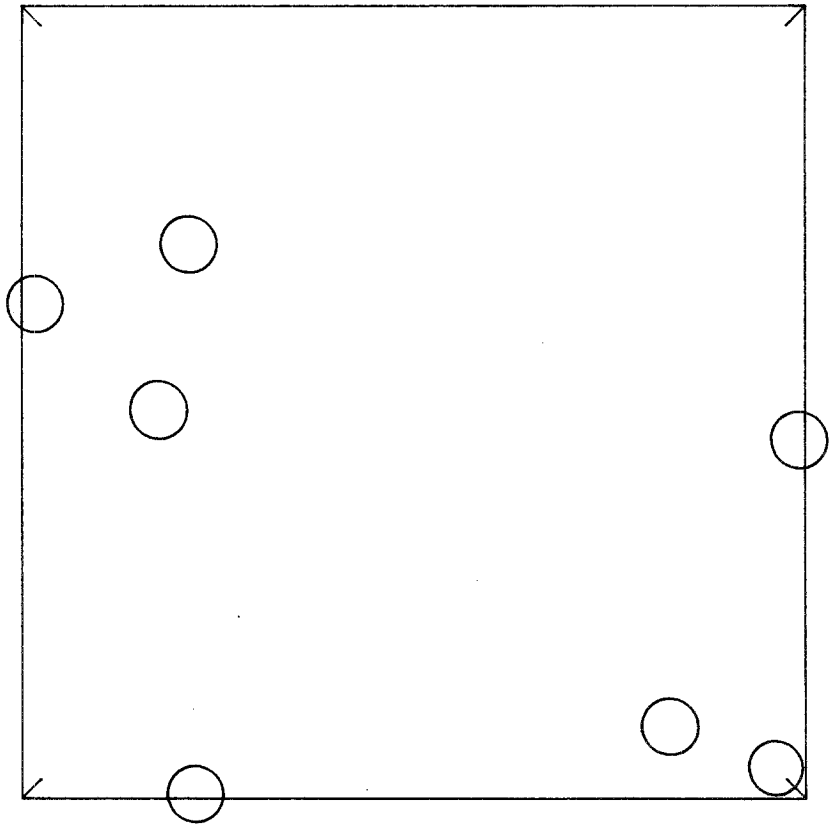

Fig. 11. Typical configuration of atoms in vapor region, centers in slab of thickness $\Delta z = 1.0$.

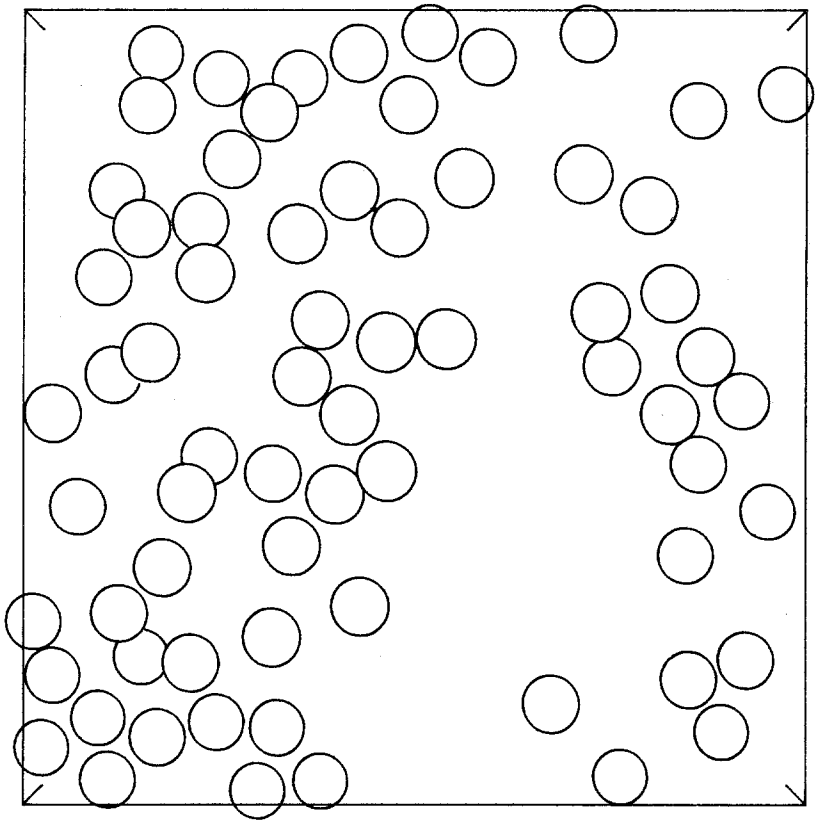

Fig. 12. Typical configuration of atoms in interface region, centers in slab of thickness $\Delta z = 1.0$.

coherence length is further perturbed by waves excited in the effectively elastic surface. Our analysis has been partly heuristic and partly rigorous, raising at least as many questions as it claims to answer. For example, the analysis of (48) applied to the density profile itself has been seen to lead to a divergence going as the logarithm of the system size. We have therefore begun a detailed study of the dynamics of the surface motions in computer simulation.

To start with, we have plotted in Figs. 11–13 the atomic configurations in the vapor, surface, and liquid regions at one particular time. Each atom is represented by a circle with diameter σ, and the partial circles represent the hidden atoms when looking from the vapor region into the surface. These pictures do show a clustering of atoms in the surface with well-defined regions of high and low density. When we follow these pictures in time, we observe the clusters moving, but it is difficult with our data to distinguish

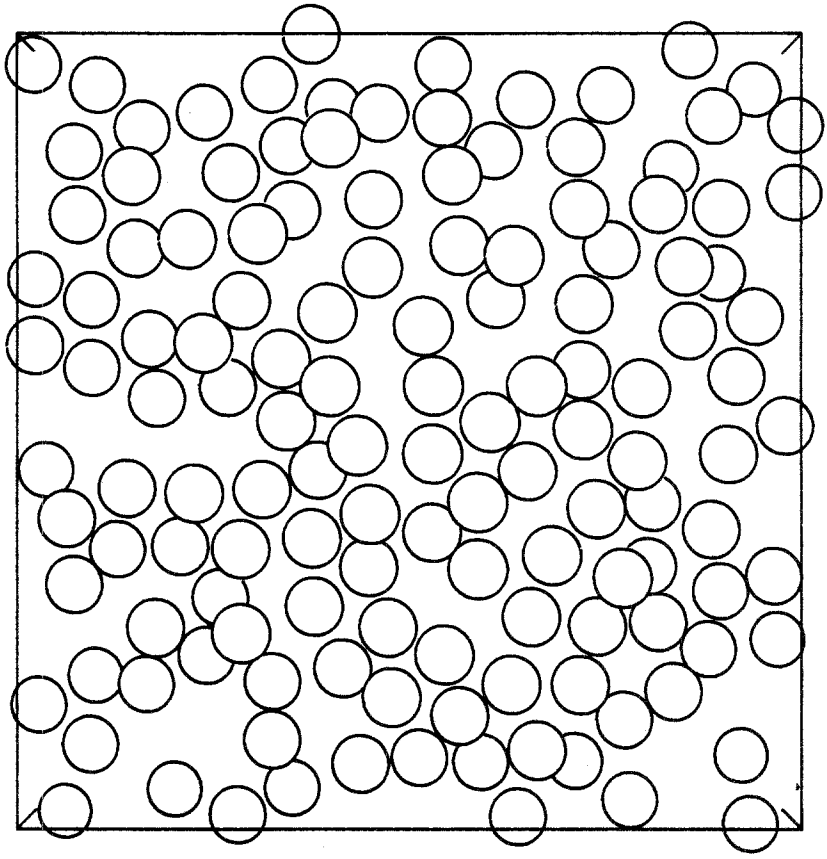

Fig. 13. Typical configuration of atoms in liquid region, centers in slab of thickness $\Delta z = 1.0$.

diffusive from wavelike propagation of the clusters. However, over as few as 800 configurations, the mean density has already achieved a form sensibly independent of x and y.

To examine the surface motion in greater detail, it is first necessary to define the surface. For a meaningful microscopic visualization, this is best done by dividing the system into gas atoms and liquid atoms. For a rather sharp criterion, we may compare the local energy of a particle with some reference energy:

$$\begin{aligned} r_i \quad &\text{in gas if} \qquad E = \sum_{j \neq i} \phi(r_i - r_j) > E_0 \\ &\text{in liquid if} \qquad\qquad\quad E < E_0 \end{aligned} \tag{57}$$

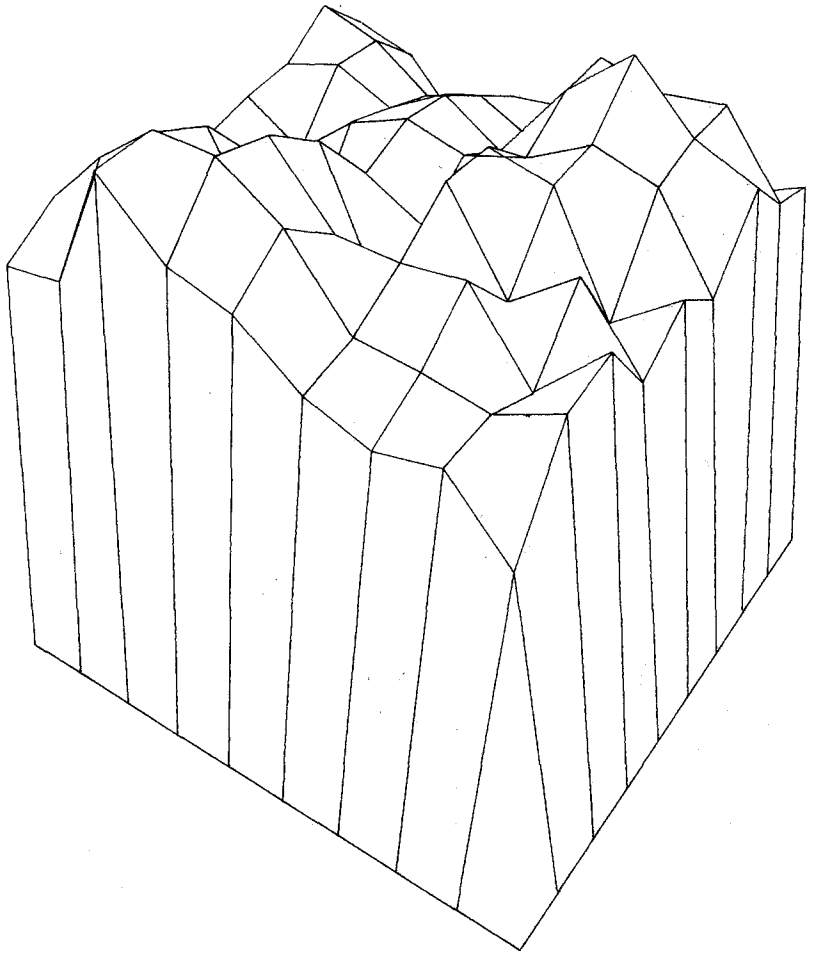

Fig. 14. Typical surface configuration of atoms with energy criterion $E_0 = 0$.

Indeed, the surface obtained from the liquid surface atom–atom connections is quite insensitive to the threshold value E_0, reinforcing the picture of a sharp short-time liquid–gas interface. This is shown in Figs. 14 and 15, essentially histograms of $\xi(x, y)$. More important is the dynamical information in the form of time-dependent correlation functions $F(\mathbf{k}, t)$, obtained by replacing $\mathbf{r}_i$ in Eq. (40) by $\mathbf{r}_i(t)$. Here, preliminary computations at least show that $F(\mathbf{k}, t)$ decays to equilibrium much more slowly in the surface region than in the bulk, evidence again of the presence of slow, long waves manifested presumably as slow, large clusters. A more detailed analysis using longer

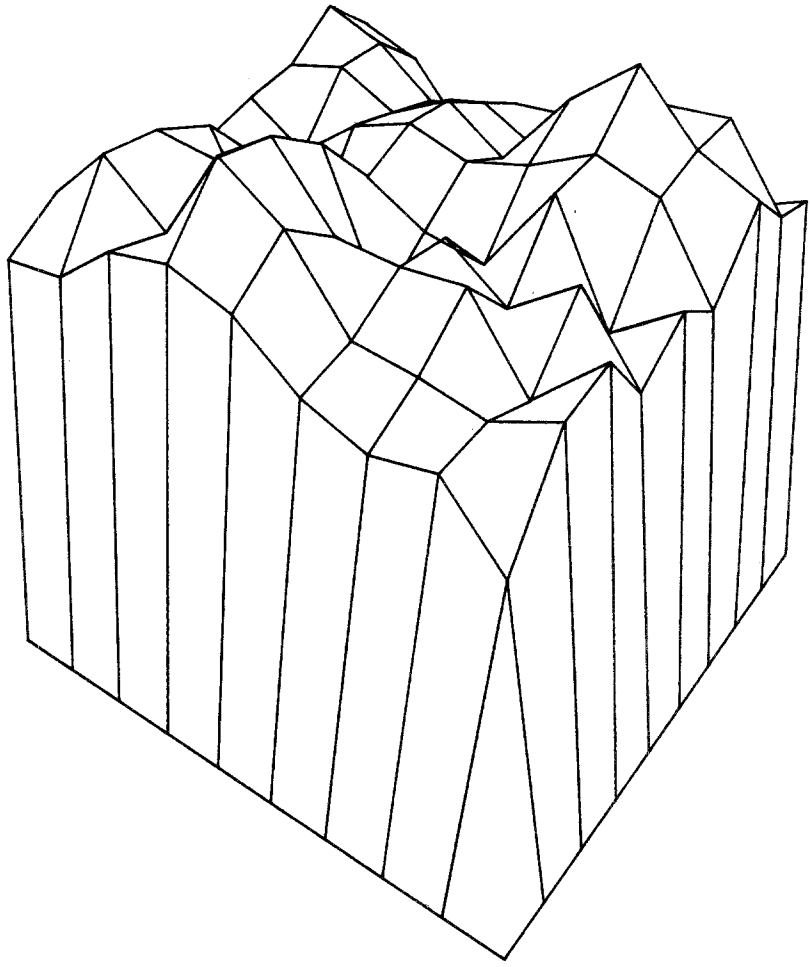

Fig. 15. Typical surface configuration of atoms with energy criterion $E_0 = -0.5$.

simulations and larger surface area is now being undertaken and will be reported in due course.

6. CONCLUSIONS

The density profile found by Rao and Levesque appears superficially to indicate a smooth and uninteresting transition from liquid to vapor extending over a broad range of about five length units. But we find as a result of the further analysis presented here that the interface has considerable structure. In particular, the transverse structure factor does not interpolate smoothly in the interfacial region. On the contrary, it exhibits a striking

peak for small k in the interface. We interpret this as evidence of capillary waves in the interface whose leading term for small k gives rise to a structure factor contribution $S(z, z'; \mathbf{k}) \propto \rho'(z)\rho'(z)$. In addition, we find that purely longitudinal correlations are consistent with a model in which the interface is taken to be planar, sharp, and fluctuating in location. Taken with the evidence provided by snapshots of atoms in the interface, we conclude that the delineation between liquid and vapor is rather abrupt—of the order of one atomic diameter for our parameters—but that this boundary fluctuates markedly in position and time.

ACKNOWLEDGMENTS

It is a pleasure to express our thanks to D. Levesque for his help in the computations, and to D. Ceperley and G. V. Chester for illuminating conversations. We are also indebted to D. Perkus for skillful programming of the graphic aids we have used.

REFERENCES

1. J. D. van der Waals, *Z. Phys. Chem. (Leipzig)* **13**:657 (1894).
2. P. S. Epstein, *Textbook of Thermodynamics* (Wiley, New York, 1937), Chapter XII.
3. K. S. Liu, *J. Chem. Phys.* **60**:4226 (1974); K. S. Liu, M. H. Kalos, and G. V. Chester, *Phys. Rev. A* **10**:303 (1974); J. K. Lee, J. A. Barker, and G. M. Pound, *J. Chem. Phys.* **60**:1976 (1974).
4. F. A. Abrahams, D. E. Schreiber, and J. A. Barker, *J. Chem. Phys.* **62**:1958 (1975).
5. M. Rao and D. Levesque, *J. Chem. Phys.* **65**:3233 (1976).
6. G. M. Nazarian, *J. Chem. Phys.* **56**:1408 (1972).
7. S. Toxvaerd, *J. Chem. Phys.* **55**:3116 (1971).
8. J. L. Lebowitz and J. K. Percus, *J. Math. Phys.* **4**:116 (1963).
9. T. L. Hill, *Statistical Mechanics* (McGraw-Hill, New York, 1956), Section 39.
10. J. K. Percus, *J. Stat. Phys.* **15**:423 (1976).
11. S. Toxvaerd, *J. Chem. Phys.* **64**:2863 (1976).
12. J. K. Percus, in *Classical Fluids*, H. L. Frisch and J. L. Lebowitz, eds. (Benjamin, New York, 1964), Appendix C.
13. D. G. Triezenberg and R. Zwanzig, *Phys. Rev. Lett.* **28**:1183 (1972).
14. R. Lovett, C. Y. Mau, and F. P. Buff, *J. Chem. Phys.* **65**:570 (1976).
15. M. S. Wertheim, *J. Chem. Phys.*, to be published.
16. F. P. Buff, R. A. Lovett, and F. H. Stillinger, *Phys. Rev. Lett.* **15**:621 (1965).
17. C. C. Chang and M. Cohen, *Phys. Rev. B* **11**:1059 (1975).
18. W. F. Saam, *Phys. Rev. B* **12**:163 (1975).